High precision measurement of the ^{19}Ne β-decay half-life using real-time digital acquisition

C. Fontbonne,[1] P. Ujić,[2] F. de Oliveira Santos,[3] X. Fléchard,[1,*] F. Rotaru,[4] N. L. Achouri,[1] V. Girard Alcindor,[3] B. Bastin,[3] F. Boulay,[3] J. B. Briand,[3] A. M. Sánchez-Benítez,[3,5] H. Bouzomita,[3] C. Borcea,[4] R. Borcea,[4] B. Blank,[6] B. Carniol,[1] I. Čeliković,[2] P. Delahaye,[3] F. Delaunay,[1] D. Etasse,[1] G. Fremont,[3] G. de France,[3] J. M. Fontbonne,[1] G. F. Grinyer,[3,7] J. Harang,[1] J. Hommet,[1] A. Jevremović,[2] M. Lewitowicz,[3] I. Martel,[5] J. Mrazek,[8] M. Parlog,[1,4] J. Poincheval,[1] D. Ramos,[9] C. Spitaels,[3] M. Stanoiu,[4] J. C. Thomas,[3] and D. Toprek[2]

[1]*Normandie Université, ENSICAEN, UNICAEN, CNRS/IN2P3, LPC Caen, 14000 Caen, France*
[2]*Vinca Institute of Nuclear Sciences, University of Belgrade, P.O. Box 522, 11070 Belgrade, Serbia*
[3]*GANIL, CEA/DRF-CNRS/IN2P3, Bvd Henri Becquerel, 14076 Caen, France*
[4]*Horia Hulubei National Institute for Physics and Nuclear Engineering, P.O. Box MG-6, 76900 Bucharest, Romania*
[5]*Departamento de Ciencias Integradas, University of Huelva, 21071 Huelva, Spain*
[6]*CENBG, 19 Chemin du Solarium, CS 10120, F-33175 Gradignan Cedex, France*
[7]*Department of Physics, University of Regina, Regina, Saskatchewan, Canada, S4S 0A2*
[8]*Nuclear Physics Institute, ASCR CZ-25068, Řež, Czech Republic*
[9]*Universidade de Santiago de Compostela, E-15706 Santiago de Compostela, Spain*

(Received 27 September 2017; published 11 December 2017)

The half-life of ^{19}Ne was measured using a real-time digital multiparametric acquisition system, providing an accurate time stamp and relevant information on the detector signals for each decay event. An exhaustive offline analysis of the data gave unique access to experimental effects potentially biasing the measurement. After establishing the influence factors impacting the measurement such as after-pulses, pile-up, gain, and baseline fluctuations, their effects were accurately estimated and the event selection optimized. The resulting half-life, $17.2569 \pm 0.0019_{(\mathrm{stat})} \pm 0.0009_{(\mathrm{syst})}$ s, is the most precise up to now for ^{19}Ne. It is found to be in agreement with two recent precise measurements and not consistent with the most recent one [L. J. Broussard *et al.*, Phys. Rev. Lett. **112**, 212301 (2014)] by 3.0 standard deviations. The full potential of the technique for nuclei with half-lives of a few seconds is discussed.

DOI: 10.1103/PhysRevC.96.065501

I. INTRODUCTION

Nuclear β decay offers an attractive electroweak process for the study of fundamental interactions [1,2] and plays an important role in nucleosynthesis, particularly in *r*-process nucleosynthesis [3] where the half-life of exotic β emitters is often a key parameter. Precise half-life measurements are also important in the investigation of the influence of electron screening on radioactive β decays [4]. During the past decade the main motivation for accurate half-life measurements of β emitters has been related to the determination of the up-down element V_{ud} of the Cabibbo-Kobayashi-Maskawa (CKM) [5,6] quark mixing matrix. The unitarity condition of the CKM mixing matrix is one of the sensitive probes to test the consistency of the three generation standard electroweak model, and any deviation from unitarity would imply new physics. The precision of this test is presently limited by the uncertainty on the value of the dominant element, V_{ud}. To date, the most precise value of V_{ud} is inferred from the so-called ft values (the product of the statistical rate function f of the transition with the partial half-life t of the decaying state) of the superallowed $0^+ \rightarrow 0^+$ pure Fermi β transitions of 14 nuclei, yielding $V_{ud} = 0.97417 \pm 0.00021$ [7]. This analysis requires, for each nucleus, a combination of high precision measurements of its Q value, of the $0^+ \rightarrow 0^+$ branching ratio, and of its half-life.

The mixed Fermi and Gamow-Teller transitions of $T = 1/2$ mirror β decays provide the second most precise value of V_{ud} [8,9]. Transitions between mirror nuclei, like in neutron decay, are induced by both the vector and axial-vector interactions, and the extraction of V_{ud} is conducted in analogy with free neutron decay. While mirror transitions offer a complementary and promising set of nuclei for the extraction of V_{ud}, they also require the additional measurement of the Fermi fractions of the transitions [10]. These are inferred from correlation measurements for a set of five $T = 1/2$ nuclear mirror transitions, leading today to $V_{ud} = 0.9728 \pm 0.0014$ [9]. The ^{19}Ne and ^{37}K nuclei hold a special place in this analysis because their decays yield the most precise contributions in the set of $T = 1/2$ nuclear mirror transitions. The uncertainty on V_{ud} is still dominated by the precision of the Fermi fraction measurements [10], but the question is raised about the reliability of the previous half-life estimation of ^{19}Ne. This is due to significant discrepancies of more than two standard deviations between the three most recent and most precise measurements: 17.262 ± 0.007 s [11], 17.254 ± 0.005 s [4], and $17.2832 \pm 0.0051_{(\mathrm{stat})} \pm 0.0066_{(\mathrm{syst})}$ s [12].

The present work reports a new high statistics measurement of the ^{19}Ne half-life whose main goal is to provide a clarification of the situation regarding the previous estimates. We also intend to demonstrate the capabilities of modern and fast real-time digital acquisition techniques, not yet commonly

*flechard@lpccaen.in2p3.fr

 ©2017 American Physical Society

used in nuclear experimental physics. To our knowledge, such acquisition systems with an effective dead time below 1 μs have been used only twice for nuclear half-life measurements [13,14]. We show here that, with appropriate precautions, relative uncertainties of 1×10^{-4} and below can be easily achieved for half-life measurements of nuclei with production rates on the order of 1×10^5 pps (particles per second). This opens up new perspectives in a context where large efforts are dedicated to improved precision in half-life measurements [4,8,11,12,15–17] and Fermi fraction measurements [9,18] to extract V_{ud} from mirror transitions. Our analysis also shows evidence for sources of systematic errors at the level of 1×10^{-4} in relative precision that *must* be addressed using a multiparametric acquisition system.

II. EXPERIMENTAL SETUP

The ^{19}Ne beam was produced at the SPIRAL1 facility of GANIL (Caen, France) by impinging $^{20}Ne^{10+}$ ions at 95 MeV/nucleon on a graphite target. The $^{19}Ne^{3+}$ ions produced within the target-Electron Cyclotron resonance (ECR) source were post-accelerated by the CIME cyclotron at $E_{\rm lab} = 5.0982$ MeV/nucleon and sent to the G2 experimental hall. The maximum beam intensity was 5×10^6 pps. To eliminate potential beam impurities from ^{19}O, a carbon stripper was introduced at the exit of the cyclotron and the ion optics downstream of the stripper was set to select the charge state 10+, larger than the maximum possible charge state of ^{19}O. The relative contamination due to ^{19}O was then measured using a silicon detector. Thanks to this effective method, this relative contamination was found to be below 1×10^{-5}.

The beam was periodically implanted in a 20×20 mm^2 50-μm-thick lead target. According to simulations, the implantation depth within the target was between 25 and 30 μm. With the reasonable assumption that the diffusion coefficient of Ne in Pb is comparable to that measured for Ne in Ag [19] and He in Au [20], the loss of Ne atoms due to diffusion out of the target was found to result in completely negligible bias on the half-life measurement. A typical half-life measurement cycle consisted of 6.4 s of beam implantation followed by 440 s of β-decay data taking. Between these two periods, the lead target was alternately moved in front of the detection system or in the beam axis using a rotating arm. The beam was on only during the implantation period. The short duration of the implantation period, about a third of the ^{19}Ne half-life, was chosen to limit the maximum count rate of the detectors below 2×10^5 counts per second. The long duration of the β-decay data-taking period, about 25 times the ^{19}Ne half-life, ensured a precise control of the background for each cycle. The detection system consisted of a 33×33 mm^2 5-mm-thick BC-400 plastic scintillator located ~5 mm away from the lead target. As shown in Fig. 1, the light from the scintillator was collected using two light guides connected to two photomultipliers (PMs; R2248 from Hamamatsu).

The signals from the two PMs were directly sent to the real-time digital acquisition system FASTER [21]. Three FASTER acquisition channels were used, each operating the digitization of the signals with a 500-MHz 12-bit converter with independent triggers based on individual thresholds. With

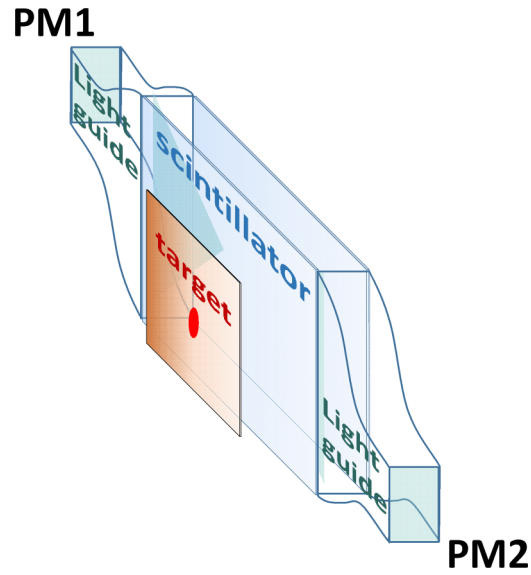

FIG. 1. Schematic view of the detection system (see text for details).

this acquisition system, the digitized frames are processed in real time by Field-Programmable Gate Array (FPGAs) using predefined algorithms adapted to the measurements to be performed [21]. All the data are time stamped with a 2-ns step, allowing online and offline correlations over user-defined time windows. For the two PMs, we chose an algorithm to process the signals from threshold to threshold: as illustrated in Fig. 2, the digital sample to be processed is selected between the crossings of the signal rising and falling edges with a threshold level defined as $th_{\rm trig}$. This choice yields samples of variable but optimal lengths with an additional dead time of only 2 ns between two successive digital data frames. For each selected frame, the algorithm provides (i) the time stamp t_i of the individual trigger with a 2-ns resolution, (ii) the threshold-to-threshold integrated charge Q_{tt}, (iii) the threshold-to-threshold duration W_{tt}, and (iv) the maximum amplitude A within a 64-ns time window following t_i and its date $t_{\rm max}$. A second-level trigger allows the events to be accepted or rejected by selecting A between the two additional thresholds $th_{\rm min}$ and $th_{\rm max}$. This second-level trigger allows

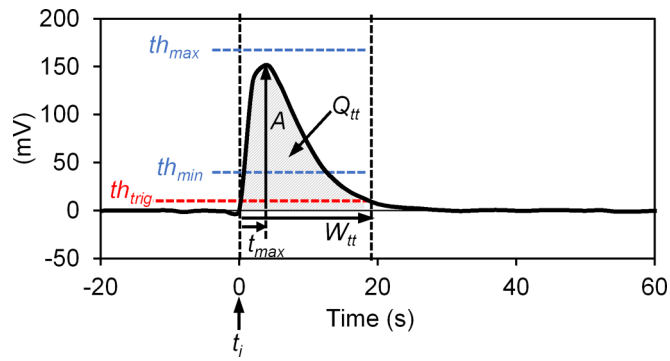

FIG. 2. Illustration of the FASTER trigger logic and recorded parameters for the PM signals (see text for details).

the use of a very low value of th_{trig} without triggering on electronic noise. An illustration of the digitization performed by the system is given in Fig. 2. In addition, the baseline of the signals was continuously monitored for each channel and corrected for low-frequency variations (below 160 kHz) by the FASTER baseline restoration algorithm. A third channel using a specific RF algorithm of FASTER was dedicated to a comparison of the internal clock of the FASTER system with an independent Oven Controlled X-tal Oscillator (OCXO) [22], whose stability and accuracy are better than 0.1 ppm (parts per million) between -55°C and 85°C. The FASTER RF module [21] was developed to perform precise measurements of the period or frequency of periodic signals such as, for instance, the frequency of a cyclotron. For each decay cycle, this module provided a measurement of the clock frequency difference with a relative precision of 9.5×10^{-9}. The average relative deviation between the two clock frequencies was found to be 8.5×10^{-7}, with maximum variations remaining below 1.6×10^{-8} throughout the entire experiment. This deviation is thus negligible with respect to the level of precision aimed in the present work.

Dead time due to the acquisition system can occur at three different stages. An intrinsic extendable dead time corresponding to the threshold-to-threshold signal duration plus 2 ns (one sample data point) is systematically present. Any other signal arising within this time window will cause pile-up and enlarge the threshold-to-threshold duration. The processing of the raw frames into calculated event data, such as that displayed in Fig. 2, is done in real time and is not subject to losses. However, if the count rate is too high (typically larger than 1×10^6 events per second), some of the data can potentially be lost as they cannot be stored in the 2-kbyte buffers of the FPGA to be sent to the acquisition computer. This possible loss of data is constantly monitored using scalers counting independently both the calculated data and the data sent to the acquisition computer. The third possible source of data loss is due to the limited writing speed of the acquisition computer hard drive. It depends on the average data flux (count rate times the number of channels times the size of the processed data) and on the performance of the hard drive. When the writing speed of the latter saturates, then a complete buffer is lost. It is thus far the dominant cause of dead time that was observed. This possible loss of data is easily detected by comparing the number of data recorded on the hard drive to the counts of data provided by the scalers of the FPGA every 1 ms. Note that, in the present experiment, a moderate detection rate was chosen so as to ensure no data losses at all besides pile-up.

III. OFFLINE DATA ANALYSIS

Compared to standard acquisition systems based on scalers, the advantages of a real-time digital multiparametric acquisition for half-life measurements of radioactive nuclei are evident. When relying on scalers, several runs using different thresholds and different hardware-imposed dead times are required to estimate the effect of pulse duration, of rate-dependent gains, or of after-pulses [11,16]. In contrast, one can here use instead a unique set of data recorded with the lowest possible threshold (20 mV for the present work) and shortest dead time (threshold-to-threshold duration). The charge (or amplitude) of the signal and the time stamp acquired for each event allow then an offline selection of the data by applying *a posteriori* the most appropriate dead time and threshold. Moreover, the charge information as a function of the time in the decay cycles and of the time interval between successive events provides the means to carefully study the sources of systematic errors and to correct for remaining gain fluctuations and pile-up effects. Such careful studies, previously discussed for the analysis of the muon half-life measurement [23], are mandatory when aiming at a relative precision better than 1×10^{-4}. However, a multiparametric acquisition system is somewhat slower than simple scalers because of the larger pieces of information to be processed and recorded. For the present experiment, the maximum instantaneous acquisition rate was limited to about 2×10^5 cps (counts per second) due to the writing speed of the acquisition computer hard drives. Nevertheless, in only 4 h of data taking comprising 33 implantation-decay cycles, $\sim 3.5 \times 10^8$ decays were recorded, yielding a relative statistical uncertainty of $\sim 1 \times 10^{-4}$.

A. Preliminary analysis and data selection

A first analysis of the data from PM1 and PM2, coupled to the 5-mm-thick scintillator, showed an average duration of the signals $\langle W_{tt} \rangle$ of 18 ns with a maximum duration of 44 ns. A nonextendable dead time of 50 ns was thus first applied to the data offline in order to impose a common and constant dead time. Figures 3 and 4 show respectively the charge and time distributions obtained for PM1 after this selection during a complete decay cycle. In Fig. 3, the charge distribution of PM1 is compared to its counterpart (labeled PM1$_{\mathrm{coinc}}$) when imposing a coincident signal from PM2 within a 16-ns time window (about twice the average rise time of the signals). This condition results in the disappearance of a large background contribution peaked at low charges. The constant-background charge distributions from PM1 signals obtained in the last 40 s of the cycle are also displayed for comparison. They

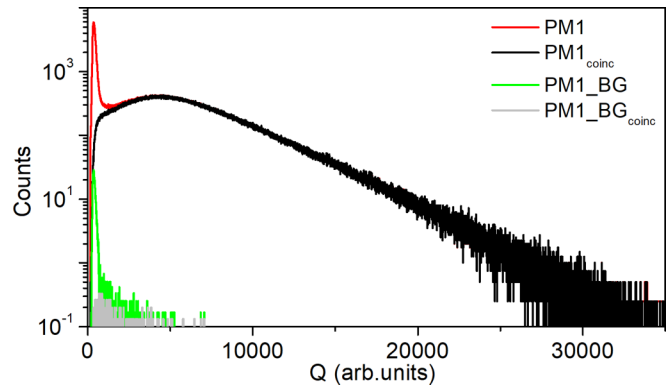

FIG. 3. Charge spectra obtained for PM1 during one full decay cycle (the first cycle) without condition (red or dark gray) and in coincidence with PM2 (black). Charge spectra obtained for the constant background of the last 40 s and normalized to a full cycle without condition (green or gray) and in coincidence with PM2 (light gray).

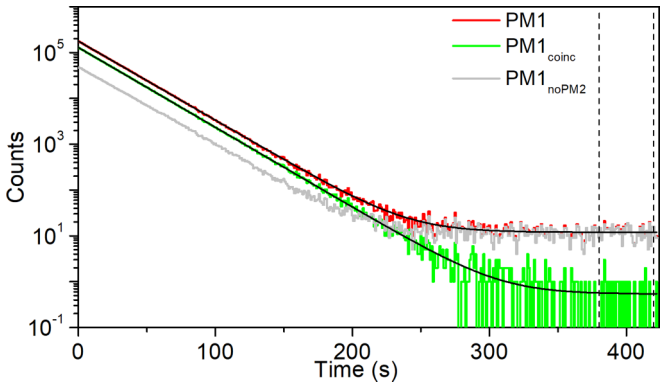

FIG. 4. Decay time spectra obtained during one decay cycle (the first cycle) for PM1 without condition (red or dark gray), in coincidence with PM2 (green or gray), and with no coincidence signal on PM2 (light gray). The bin width of the histogram is 1 s. The fit functions are plotted as black lines. The time window used for constant background selection is indicated by vertical dashed lines.

were previously normalized to the complete cycle duration. The typical rate of the PM1 constant-background was about 12 s^{-1} without coincidence and below 0.5 s^{-1} in coincidence with PM2. In both cases, the constant-background contribution yields only signals with low charges. Figure 4 shows the time spectra obtained for PM1 signals, for PM1 signals detected in coincidence with PM2 (labeled $PM1_{coinc}$), and PM1 signals detected without triggering PM2 (labeled $PM1_{noPM2}$). The latter selection of events corresponds to the background peak at very low charge observed in the red curve of Fig. 3. For these background events, the time dependence shown in Fig. 4 is very similar to that of events obtained in coincidence. This source of background strongly correlated to the decay rate was therefore attributed mostly to after-pulses and Cerenkov light emitted from the light guide or from the PM structure, and possibly to scattered or very low-energy β particles and photons triggering only one PM. The experimental data of Fig. 4 obtained for PM1 and $PM1_{coinc}$ were fitted using the decay function:

$$D_{neDT}(t) = \frac{D(t)}{1 + neDT \times D(t)} \tag{1}$$

with $D(t) = D_0 e^{(-t/\tau)} + BG$, where D_0 is the initial decay rate, $\tau = T_{1/2}/\ln(2)$ the decay time constant, BG the constant background rate, and $neDT$ the nonextendable dead time of 50 ns imposed by software. The fit method was based on likelihood maximization for data following the Poisson distribution. To avoid any influence of the bin width chosen for the construction of the time decay spectra, the actual fit function applied to the histograms takes the form

$$F_{neDT}(t_i) = \int_{t_i - \frac{\Delta t}{2}}^{t_i + \frac{\Delta t}{2}} D_{neDT}(t)\, dt, \tag{2}$$

where Δt is the bin width, i is the bin number, and $t_i = i\,\Delta t + \frac{\Delta t}{2}$.

At this stage of the analysis, the reduced χ^2 of 671.0 for 421 degrees of freedom (424 bins of 1 s and three free parameters) obtained for the raw PM1 data, with a P value

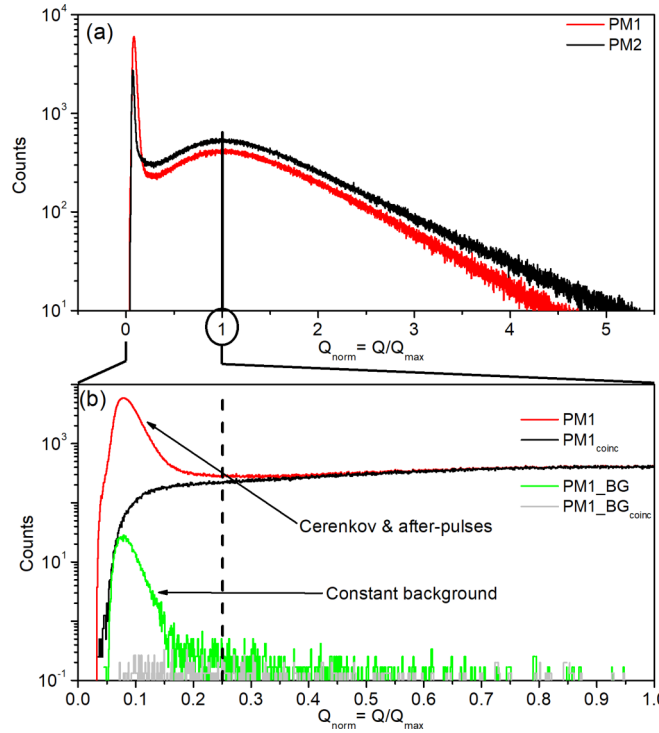

FIG. 5. Charge spectra obtained during the first decay cycle for (a) PM1 (red or dark gray) and PM2 (black) after normalization. The enlarged view (b) also shows the charge distribution for $PM1_{coinc}$ (black) and the constant background contributions (green or gray, and light gray). A threshold $Q_{th} = 0.25$ is indicated by the vertical dashed line.

below 1×10^{-4}, already indicates a disagreement with the model decay function. However, the reduced χ^2 of 434.1 for PM1 data in coincidence with PM2 corresponds to a P value of 0.32, which does not allow questioning the model function or the data selection. As for experiments using a "standard" acquisition, it is now still required to look for an optimum threshold and dead time. For each cycle, the positions Q_{max} of the maximum of the charge distributions of PM1 and PM2 were determined using a polynomial function of third degree. All the charge spectra were then normalized, as illustrated in Fig. 5(a), using the observable $Q_{norm} = Q_{tt}/Q_{max}$. This independent normalization for each cycle and the two PMs provides a common reference for applying a software threshold in charge Q_{th}. As was done in Fig. 3, Fig. 5(b) shows the contributions from constant background and from Cerenkov or after-pulses triggering only PM1. It already indicates that a minimum threshold close to $Q_{th} = 0.25$ has to be applied on the charge Q_{norm} after normalization.

An important feature of the acquisition system is the time stamping of the data. By providing a precise time for each event, it is possible to look at the decay events as a function of the time interval θ between successive triggers. The advantages of an analysis based on time-interval distributions were previously presented in Ref. [24]. Here, we use this information to optimize the data selection. Figure 6 shows the time-interval histograms obtained with PM1 for one cycle when applying different thresholds on the charge

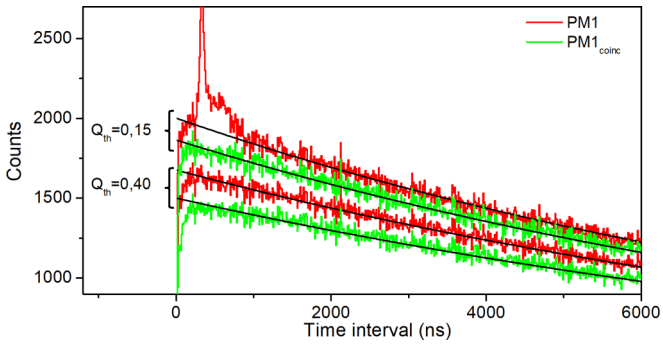

FIG. 6. Time-interval spectra obtained for the first decay cycle with PM1 (red or dark gray) and coincidences (green or gray) using thresholds in charge $Q_{\text{th}} = 0.15$ and $Q_{\text{th}} = 0.40$. Theoretical distributions are given by black lines. The bin width of the histogram is 10 ns.

after normalization. They are compared to the theoretical distribution expected with no dead time [25]:

$$H(\theta) = \tau e^{-BG\theta}\left[\frac{e^{-D_e\theta} - e^{-D_0\theta}}{\theta} + BGEi(-D_0\theta) - BGEi(-D_e\theta)\right], \quad (3)$$

where Ei is the exponential integral function, $D_e = D_0 e^{(\frac{-T_e}{\tau})}$, T_e is the duration of the cycle, and the parameters BG, D_0, and τ are inferred from a fit of the decay time distribution. For PM1 data and a threshold $Q_{\text{th}} = 0.15$, large deviations due to after-pulses are clearly visible, indicating a minimum appropriate offline dead time of $\sim$1.0 μs. For PM1 data in coincidence with PM2 and higher thresholds, a deficit of counts below 1 μs is also observed. This can be attributed to other effects correlated with count rate such as pile-up, baseline, and detector gain variations. Beyond these observations, the other obvious advantage of the time-stamp information is that an appropriate constant and precise dead time can be applied to the data afterward, by selecting events separated by a minimum difference in detection time. In the following analysis, we used a conservative software imposed dead time $neDT = 1.5$ μs resulting in a negligible loss of statistics. This selection, combined with the use of Eq. (1) with the corresponding $neDT$ value, suppresses the bias associated to after-pulses and accounts for missing data due to pile-up.

B. Systematic effects

After having estimated the appropriate minimum dead time and threshold, additional systematic effects such as gain variations, baseline variations, and second order effects due to pile-up were studied. During two short runs, each consisting of one decay cycle, the FASTER acquisition was used in an "oscilloscope mode," providing frames of 2.8 μs duration recorded at a 1-kHz rate. One run of 100 s duration was recorded with a high initial detection rate of $\sim$1 Mcps and another run of 50 s duration with a moderate initial detection rate of $\sim$150 kcps, comparable to the experimental conditions for the 33 implantation-decay cycles. These oscilloscope

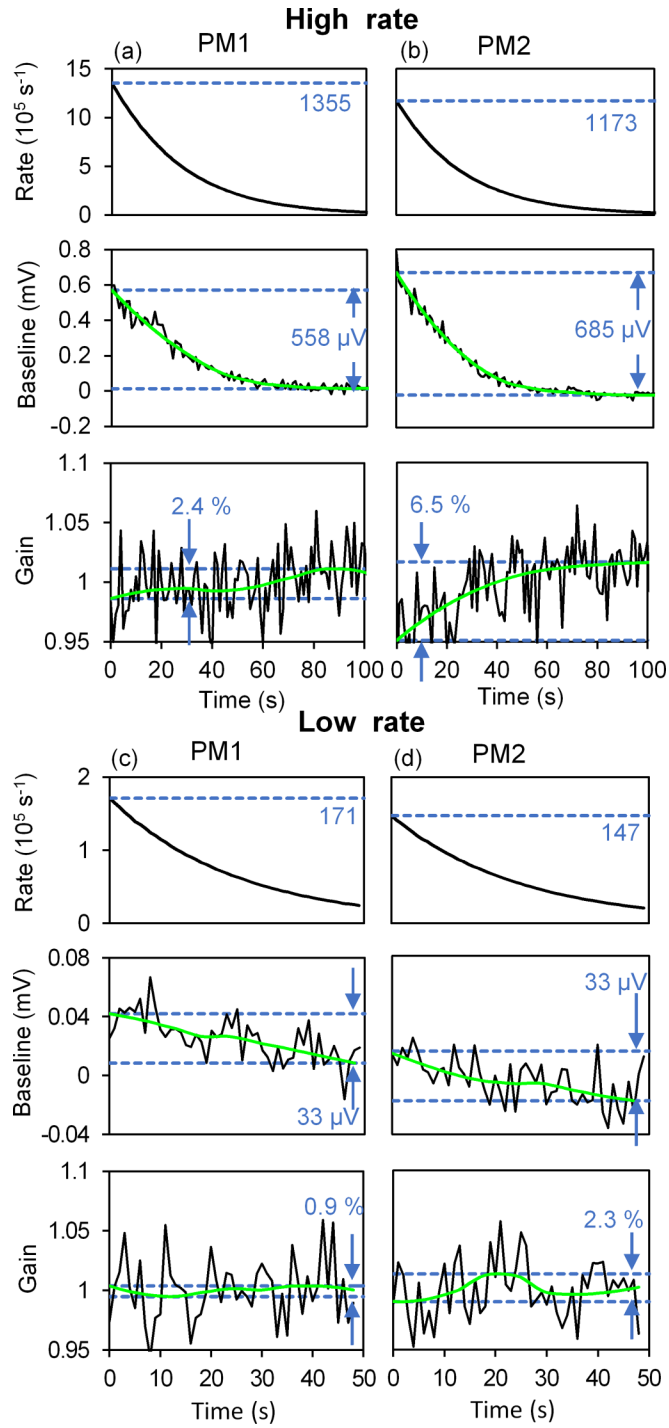

FIG. 7. Count rates, baseline variations, and gain variations inferred from oscilloscope frames for PM1 and PM2 at $\sim$1 Mcps and $\sim$150 kcps initial rates. Fluctuations due to the limited statistics are smoothened using a LOESS regression (LOcal regrESSion) from the R software package [26] (green or gray line).

frames were analyzed offline in order to estimate the baseline and the mean charge $\langle Q_{tt}\rangle$ of the signals as a function of time within a cycle. Changes of $\langle Q_{tt}\rangle$ with time were then interpreted as gain variations of the detection system. The results of this analysis for the four cases are displayed in Fig. 7.

The baseline variations are found to be strongly correlated with the instantaneous decay rate. The gain variations are more difficult to interpret. For PM2 and for an initial detection rate of ∼1 Mcps, it follows approximately an exponential growth with a time constant comparable to the nuclear decay one. For the three other cases, the gain oscillates without obvious pattern. For the ∼150 kcps initial rate, we found gain and baseline variations with amplitudes of respectively 0.9% and 33 μV for PM1 [Fig. 7(c)], and 2.3% and 33 μV for PM2 [Fig. 7(d)]. For the high initial rate, it becomes 2.4% and 558 μV for PM1 [Fig. 7(a)], and 6.5% and 685 μV for PM2 [Fig. 7(b)]. This indicates stronger variations with higher rates, and a better stability of PM1 compared to PM2. The variations of the baseline, similar for both PMs, could be interpreted as resulting from a small exponential decay tail in the PM signals each time a β is detected. This tail has a typical initial amplitude of $V_{\text{tail}} \sim 100$ μV and decays with a time constant of $\tau_{\text{tail}} \sim 5$ μs that is too short to be properly corrected by the FASTER baseline restoration algorithm.

The resulting baseline corresponds to the convolution of this exponential decay function with a Dirac comb of period inversely proportional to the decay rate:

$$BL(t,D_0) = V_{\text{tail}} \frac{e^{-\frac{1}{\tau_{\text{tail}} D_0 e^{(-t/\tau)}}}}{1 - e^{-\frac{1}{\tau_{\text{tail}} D_0 e^{(-t/\tau)}}}} + V_0, \tag{4}$$

where V_0 is the constant baseline at zero decay rate. The parameters V_{tail}, τ_{tail}, and V_0 were extracted from a fit of the oscilloscope frames for PM1 and PM2. This modeling of the baseline variation was found to be in excellent agreement with the oscilloscope data.

These effects, by changing the shape of the charge distribution as a function of time, modify the probability of accepting an event when applying a charge threshold and therefore affect the resulting decay time spectra. In a similar way, pile-up events whose probability is correlated with count rate modify the shape of the charge distribution with time. This second order effect is not taken into account in the dead time correction performed by Eq. (1). The impact of these variations on the time decay spectrum obtained after applying a charge threshold Q_{th} has been thoroughly studied using a dedicated numerical model. The details of this work can be found in Ref. [25]. It will be the object of a separate publication and only the main components are given in the following. The numerical data were generated using the signal duration W_{tt} and charge Q_{norm} density functions of the experimental events. These density functions were obtained after applying a nonextendable dead time $neDT = 1.5$ μs to the data, by selecting decay events where pile-up is expected to be negligible, and after subtraction of the constant-background contribution extracted from the last 40 s of each cycle. In our model, gain and baseline variations were then applied numerically to the charge using an exponential time dependence. To simulate the effect of gain variation, the initial charge Q_{norm} was multiplied by a factor $G(t)$ given by

$$G(t) = 1 - \Delta G_0 e^{-\frac{t}{\tau}}, \tag{5}$$

where ΔG_0 is the maximum gain variation. Note that, in this study, we chose a gain variation model similar to the one observed for PM2 at ∼1 Mcps initial count rate. Then, we added the charge offset due to the baseline fluctuation given by

$$Q_{\text{offset}}(t) = BL(t,D_0) W_{tt}, \tag{6}$$

where W_{tt} is the duration of the signal and $BL(t,D_0)$ the baseline modeled by Eq. (4). The effect of pile-up on the recorded charge distribution was also accounted for by using a convolution of two charge distributions obtained when pile-up is negligible. The fraction of the charge spectrum resulting from pile-up events is then defined as

$$p_e(i) = 1 - e^{-W_{tt}\frac{N_i}{\Delta t}}, \tag{7}$$

where N_i is the number of events detected in a given interval of time Δt.

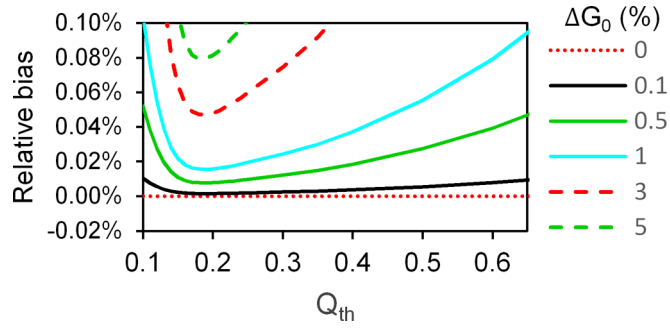

FIG. 8. Expected relative bias on the half-life estimation for PM1 due to gain variations as a function of the threshold Q_{th}.

Using this numerical model, a systematic study of the bias on the half-life estimation induced by gain and baseline variations as well as pile-up was then performed as a function of the threshold Q_{th} chosen for data selection. Figure 8 shows the expected relative bias for PM1, resulting from gain variations with different values of ΔG_0. Similar results, not shown here, were obtained for the signals of PM2. Even for small gain variations with $\Delta G_0 = 1\%$, we find a relative bias of 1.6×10^{-4} at the optimal threshold, close to $Q_{\text{th}} = 0.2$. This bias increases almost linearly with ΔG_0. It also increases strongly when moving Q_{th} away from optimum. This shows that without an extremely stable PM gain (stability better than 1%), a relative precision at the level of 1×10^{-4} requires gain monitoring and an appropriate selection of charge threshold. Note that for a gain variation of 6.5%, as obtained with PM2 at high rates, the expected minimum relative bias is close to 1×10^{-3}, far above the 1×10^{-4} statistical relative uncertainty of the present data. Similarly, the effects of pile-up and of baseline variations for several initial detection rates and as a function of the threshold Q_{th} are given in Fig. 9. As for the gain variation, a charge threshold Q_{th} close to 0.25 strongly reduces the bias. With this threshold and the detection rates of the present experiment (between 150 and 200 kcps), the expected relative bias due to baseline variation is -1.0×10^{-5} and the one due to pile-up is -0.6×10^{-5}, with errors on these estimates below 1×10^{-6}. However, running at a 1 Mcps initial rate would have induced a minimum relative bias of $\sim -1 \times 10^{-4}$ due to baseline variation and of $\sim -3 \times 10^{-5}$ due to pile-up. From these results, it is clear that for a

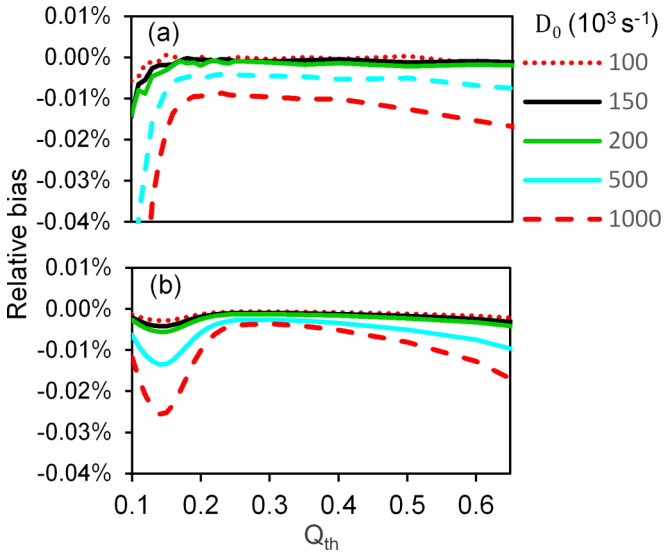

FIG. 9. Expected relative bias on the half-life estimation for PM1 signals, due to (a) baseline variations and (b) pile-up as a function of the threshold Q_{th} for different initial rates D_0.

1 Mcps initial detection rate the gain and baseline variation effects discussed above can cause systematic errors larger than 1×10^{-4}. For the lower rate, the impact of pile-up and of baseline variations is negligible, but the relative bias induced by gain fluctuations as simulated in our model was found to be of the order of 1×10^{-4}.

To compare the model to real data, we applied the same procedure using the gain variations of Fig. 7 obtained during the unique cycle dedicated to oscilloscope frames and recorded with a ∼150 kcps initial detection rate. The half-lives as a function of Q_{th} given by the model with PM1 and PM2 charge distributions are shown in Fig. 10. It assumes a nonbiased initial half-life of 17.2569 s, which is the final result of our analysis. It is compared to the experimental results given by the weighted average of the 33 time decay values, obtained by fitting the decay time spectra of PM1 and PM2 data with Eq. (2). The data were filtered beforehand by applying a

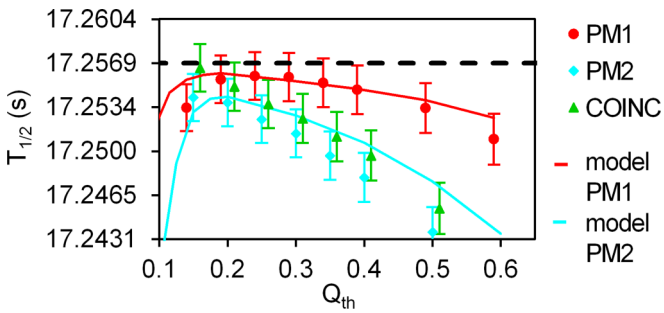

FIG. 10. Half-lives as a function of Q_{th} given by the model with PM1 and PM2 charge distributions using gain variations from Fig. 7 (lines), compared to half-lives resulting from the fit of the 33 time decay curves obtained with PM1, PM2, and coincidence experimental data (points). The horizontal dashed line indicates the final value of the half-life resulting from the present analysis (see text for details).

nonextendable dead time of 1.5 μs and the thresholds Q_{th} indicated on the horizontal axis. The half-lives obtained for data corresponding to coincidences between PM1 and PM2 are also shown. Despite the fact that the gain fluctuations occurring during the 33 decay cycles may have been different than the gain fluctuations measured with our single oscilloscope run, we observe a good agreement between the model and the experimental data. Minimum relative bias of 5×10^{-5} and 1.2×10^{-4}, for PM1 and PM2, respectively, are obtained for Q_{th} close to 0.25 for PM1 and 0.2 for PM2. The dependence of the bias to Q_{th} follows a pattern similar to that of Fig. 8, but with opposite sign. This is due to the shape of the gain variations obtained with the oscilloscope data at a low rate that differs from the exponential growth previously considered in the model. One can also note that selecting PM signals in coincidence does not reduce the bias. On the contrary, Fig. 10 shows that for most values of Q_{th}, the selection of coincidence events results in a bias close to the one obtained for PM2 data (more affected by gain fluctuations) that is larger than for PM1 data alone.

C. Event-by-event compensation and final results

In spite of the apparent good agreement obtained when using the oscilloscope data to model the effect of gain fluctuations, a more robust analysis requires access to gain fluctuations occurring along each decay cycle. For the final analysis of the data, a gain compensation algorithm was thus developed. The decay time spectrum of each cycle was first divided into time intervals containing 5×10^3 events. Using the mean charge recorded during these intervals and a recursive procedure [25], the gain variation from one interval to another was inferred. In this procedure, the negligible effect of the ∼30 μV baseline variation was not accounted for. The gain variations were then compensated on an event-by-event basis, prior to applying the charge threshold. The decay time spectra were eventually fitted using Eq. (2) with a nonextendable dead time of 1.5 μs. Three different minimization methods were used: the Newton method from the R statistical computing package, the Levenberg-Marquardt algorithm, and the quasi-Newton method from MIGRAD, all yielding the same result. The half-lives obtained that way for PM1, PM2, and coincidence events with different charge thresholds Q_{th} are given in Fig. 11. After compensation for gain variations, the half-life estimations obtained with PM1 become very weakly dependent on the threshold Q_{th} and remain constant from $Q_{\text{th}} = 0.2$ to $Q_{\text{th}} = 0.4$. For PM2 data, more affected by gain variations, the gain compensation effect is less effective. The half-life estimations obtained for the optimal threshold, close to $Q_{\text{th}} = 0.2$, are in good agreement with PM1 data but the compensation does not completely correct for the deviations observed with higher thresholds. This limitation was attributed to the available statistics when measuring gain fluctuations along the cycles. The procedure allows one to measure gain variations with a statistical uncertainty still better than the correction itself only up to 140 s in the decay cycle. For PM2, gain fluctuations beyond 140 s within the cycles, not accessible here, still impact the data. As a consequence, we only kept the result obtained

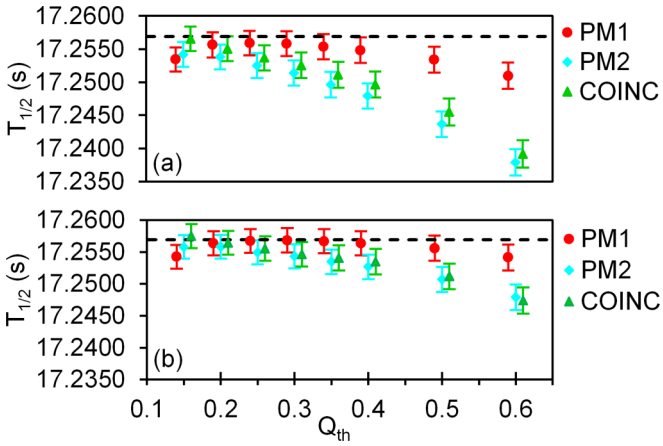

FIG. 11. Half-lives as a function of Q_{th} obtained for PM1, PM2, and coincidences (a) before and (b) after applying the gain compensation algorithm. The horizontal dashed lines indicate the final estimation of the half-life based on the present analysis (see text for details).

with PM1 at the optimum threshold $Q_{th} = 0.25$, yielding the estimate $T_{1/2} = 17.2569 \pm 0.0019_{(stat)}$ s after including the small aforementioned corrections for pile-up and baseline variations.

The partial failure of the gain compensation algorithm for PM2 motivated further studies to estimate potential systematic errors induced by the compensation. This was done by means of Monte Carlo (MC) simulations of 100 cycles with statistics comparable to the experimental data. For the time distribution, we used Eq. (1) with a nonextendable dead time of 1.5 μs, $T_{1/2} = 17.2569$ s, and values of D_0 and BG equal to the ones inferred from experimental data. For the charge distribution, the experimental data of PM1 signals were directly used. The simulations were performed without gain variation along the cycles' duration. Then, the procedure to measure and correct gain variations was applied to the MC data. The relative error on the gain measurement due to the limited statistics remained below 0.6% and resulted in a systematic error on the half-life estimation $\Delta T_{1/2(syst)} = 0.0009$ s.

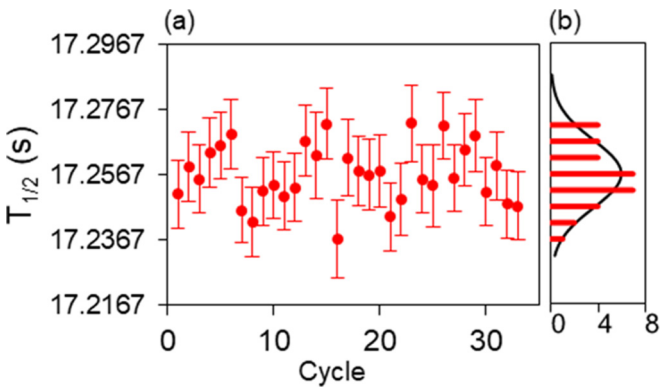

FIG. 12. (a) Half-life estimations with PM1 for the 33 cycles using $Q_{th} = 0.25$ gain compensation. (b) Normalized residuals distribution.

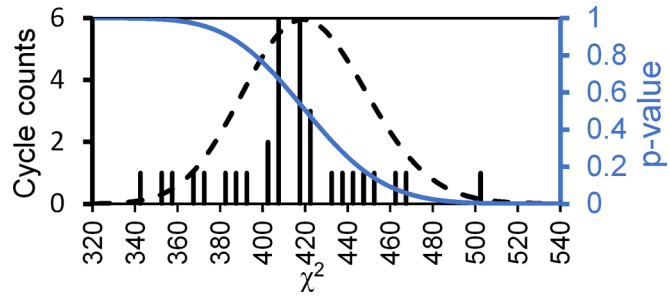

FIG. 13. χ^2 distribution of the 33 cycles using PM1 data, $Q_{th} = 0.25$, and gain compensation. The associated P values and the shape of the theoretical χ^2 distribution (black dashed line) are also indicated for 421 degrees of freedom.

Software-applied dead times ranging from 1 to 4 μs were also investigated, showing no significant effect besides the additional loss of statistics. Similarly, the dependence on initial count rate was also studied by changing the lower limit of the fit applied to the time decay spectra. Again, no notable variation of the half-life estimation resulted from these tests. As shown in Fig. 12, the half-lives obtained by fitting each cycle individually were statistically consistent, without any trend indicating a slow drift along the complete duration of the experiment. The χ^2 distribution obtained for PM1 with the 33 cycles, shown in Fig. 13, is perfectly compatible with the one expected for 421 degrees of freedom.

Our final estimation of the half-life of ^{19}Ne, $T_{1/2} = 17.2569 \pm 0.0019_{(stat)} \pm 0.0009_{(syst)}$ s, is found in perfect agreement with the former measurements of Triamback *et al.* [11] and Ujic *et al.* [4], as illustrated in Fig. 14. However, it differs by 3.2 standard deviations from the value obtained by Broussard *et al.* [12] and tends to discard the latter. Despite the rigorousness of the Broussard and collaborators analysis, the total contribution of the numerous corrections, all at the 1×10^{-4} level, that were applied (for dead time, accidental coincidences, diffusion, background, and contamination) may have been underestimated.

D. Warnings

We showed in the previous section that gain variations, baseline variations, and pile-up can affect a decay time spectrum and result in a significant bias for half-life estimations. When aiming at a relative precision of 1×10^{-4} or below,

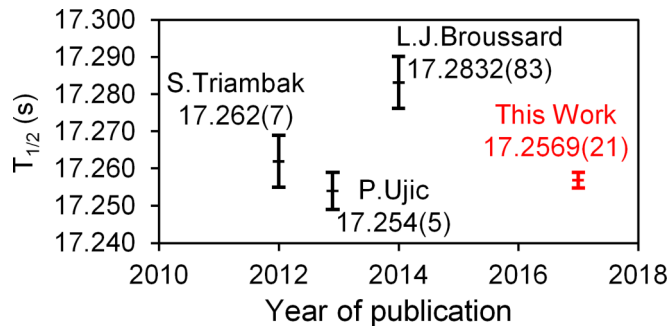

FIG. 14. Most recent and precise measurements of ^{19}Ne half-life.

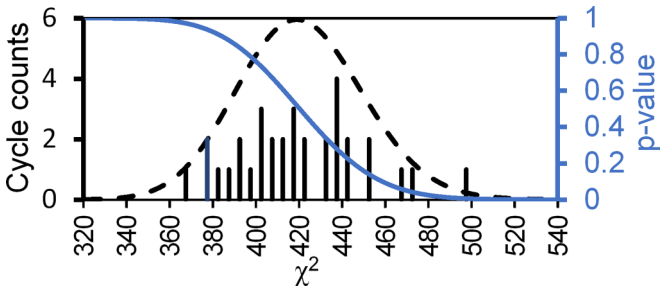

FIG. 15. χ^2 distribution of the 33 cycles using PM2 data, $Q_{\text{th}} = 0.6$, and no gain compensation. The associated P values and the shape of the theoretical χ^2 distribution (dashed black line) are also indicated for 421 degrees of freedom.

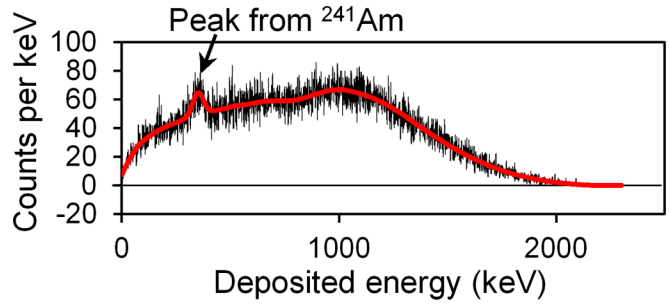

FIG. 16. Simulation of the deposited energy spectrum in a 5-mm-thick BC400 scintillator irradiated by 2.5×10^5 β particles from ^{19}Ne decay and 1×10^3 α particles from ^{241}Am. The horizontal axis indicates the energy in keV electron equivalent.

pile-up and baseline fluctuations seem to remain negligible for the moderate initial count rates chosen for the present work but may become significant for rates of $\sim$1 Mcps and higher. The impact of gain fluctuations was found to be more critical, as even for small variation of the order of 1% and an optimal threshold, a relative bias of the order of $\sim 1 \times 10^{-4}$ can be expected. To detect such a bias without dedicated measurements, one can only rely on a verification of the χ^2 distribution and hope that it is sensitive to this systematic effect. As shown in Fig. 11(a), the half-life estimation obtained for PM2 without gain compensation when applying a threshold $Q_{\text{th}} = 0.6$ is about nine standard deviations away from our final result. Figure 15 shows the associated χ^2 distribution for the 33 cycles. It is still perfectly compatible with what one would expect for 421 degrees of freedom. Similar χ^2 distributions (not shown here) were obtained for all the results given by Fig. 11(a), despite large disagreements between these biased half-life estimations and the final one. We can thus conclude that with the present statistics yielding relative statistical uncertainties of $\sim 1 \times 10^{-4}$, the χ^2 test does not allow one to detect a relative bias due to gain variation smaller than $\sim 1 \times 10^{-3}$. By contrast, the systematic study of the decay spectrum as a function of charge threshold performed in the present analysis was found to be very sensitive to such sources of bias.

IV. FUTURE IMPROVEMENTS

To improve the relative precision of $\sim 1 \times 10^{-4}$ obtained with the present measurement, several simple upgrades can be foreseen. The main limitations were here due to statistics. With 2 days of beam time (instead of only 4 h) and a second detector to double the solid angle, a gain of a factor of $\sim$24 can readily be obtained. The initial event rate per channel can be easily increased by a factor of 2 without data losses in the acquisition by using two hard drives with higher writing speed. Other minor improvements can also be performed by optimizing the cycle duration (gain of a factor of $\sim$1.2) and by limiting the Cerenkov contribution in the light guides (gain of a factor of $\sim$1.3). The overall gain in statistics would lead to a relative statistical error of $\sim 1 \times 10^{-5}$. Note that such a statistics is accessible in a reasonable time only by using fast detectors, such as scintillators, and with beam intensities of the order of a few 10^5 pps.

At this level of precision, pile-up, baseline, and gain fluctuations have to be considered very carefully. The bias due to pile-up, on the order of $\sim 1 \times 10^{-5}$, can be estimated with a relative precision better than 1×10^{-6} thanks to the knowledge of the Q_{tt} and W_{tt} distributions. The effect of baseline variations was also precisely estimated in the present work, thanks to the oscilloscope data and a variation only correlated to the detection rate. One could, however, benefit from a measurement of the baseline for each detected event by using an additional charge integration window just before the trigger. The FASTER system readily allows the use of such a window within the 20 ns preceding the trigger and this feature will be implemented in the future versions of the acquisition.

The gain variation is more problematic as (i) the associated minimum bias was at the level of 1×10^{-4} for the present experiment and (ii) the relative error on the gain measurement was limited to 0.6%, yielding a relative systematic error of 5×10^{-5} on the half-life estimate. A promising improvement consists in using a monochromatic calibration source during the half-life measurement. Figure 16 shows the expected charge spectrum obtained in 1 s with a scintillator irradiated by 2.5×10^5 β particles from ^{19}Ne decay and α particles from a 2 kBq ^{241}Am source. Because of quenching, the light produced by the 5.5 MeV α particles corresponds to the light emitted by $\sim$350 keV β particles. Considering a 10% energy resolution at 1 MeV for β particles and a ^{241}Am activity of 20 kBq, the expected precision on gain monitoring for 1 s using the mean position of the α peak is 0.07%. This would reduce the relative error due to gain variations on the half-life estimate below 7×10^{-6}. Another approach would consist in limiting the intrinsic gain variation of the detection setup. For this purpose, it is now also foreseen to test the replacement of the PMs by silicon photomultipliers, whose stability could be better.

V. CONCLUSION

Thanks to a real-time digital multiparametric acquisition system, the half-life of ^{19}Ne has been measured with the unprecedented relative precision of 1.2×10^{-4}. The result, in agreement with the measurements of Triambak *et al.* and Ujic *et al.* [4,11], is not consistent with the last measurement by Broussard *et al.* [12]. The detailed analysis of the data provided by the multiparametric acquisition system has shown

that at this level of precision, pile-up, baseline variations, and primarily gain variations have to be considered carefully. Recording additional parameters such as integrated charge and absolute time stamp allows one to both determine the optimal dead time and threshold and to check the conformity of the model decay function. It was also demonstrated that a study of the decay time dependence on the charge threshold is very sensitive to bias that cannot be revealed by a χ^2 test. Several possible improvements have been discussed, showing that relative precisions of the order of 1×10^{-5} can be achieved for half-life measurements of nuclei with production rates above 1×10^5 pps.

ACKNOWLEDGMENTS

We would like to express our gratitude to the GANIL crew for delivering the radioactive beams and for friendly collaboration. We acknowledge the support of European ENSAR project cycles (No. 262010), from French-Romanian Collaboration Agreement IN2P3-IFIN-HH Bucharest No. 03-33, the Région of Basse Normandie, Helmholtz Association (HGF) through the Nuclear Astrophysics Virtual Institute (NAVI) and LEA IN2P3-ASCR NuAG projects and Ministry of Education, Science and Technological Development of Serbia—Project P171018. We thank Oscar Naviliat-Cuncic for useful discussions.

[1] B. R. Holstein, J. Phys. G **41**, 114001 (2014).
[2] N. Severijns, J. Phys. G **41**, 114006 (2014).
[3] M. Arnould, S. Goriely, and K. Takahashi, Phys. Rep. **450**, 97 (2007).
[4] P. Ujić, F. de Oliveira Santos, M. Lewitowicz, N. L. Achouri, M. Assie, B. Bastin, C. Borcea, R. Borcea, A. Buta, A. Coc, G. de France, O. Kamalou, J. Kiener, A. Lepailleur, V. Meot, A. Pautrat, M. G. Saint Laurent, O. Sorlin, M. Stanoiu, and V. Tatischeff, Phys. Rev. Lett. **110**, 032501 (2013).
[5] N. Cabibbo, Phys. Rev. Lett. **10**, 531 (1963).
[6] M. Kobayashi and T. Maskawa, Prog. Theor. Phys. **49**, 652 (1973).
[7] J. C. Hardy and I. S. Towner, Phys. Rev. C **91**, 025501 (2015).
[8] J. Grinyer, G. F. Grinyer, M. Babo, H. Bouzomita, P. Chauveau, P. Delahaye, M. Dubois, R. Frigot, P. Jardin, C. Leboucher, L. Maunoury, C. Seiffert, J. C. Thomas, and E. Traykov, Phys. Rev. C **91**, 032501(R) (2015).
[9] B. Fenker *et al.*, arXiv:1706.00414.
[10] O. Naviliat-Cuncic and N. Severijns, Phys. Rev. Lett. **102**, 142302 (2009).
[11] S. Triambak, P. Finlay, C. S. Sumithrarachchi, G. Hackman, G. C. Ball, P. E. Garrett, C. E. Svensson, D. S. Cross, A. B. Garnsworthy, R. Kshetri, J. N. Orce, M. R. Pearson, E. R. Tardiff, H. Al-Falou, R. A. E. Austin, R. Churchman, M. K. Djongolov, R. D'Entremont, C. Kierans, L. Milovanovic, S. O'Hagan, S. Reeve, S. K. L. Sjue, and S. J. Williams, Phys. Rev. Lett. **109**, 042301 (2012).
[12] L. J. Broussard, H. O. Back, M. S. Boswell, A. S. Crowell, P. Dendooven, G. S. Giri, C. R. Howell, M. F. Kidd, K. Jungmann, W. L. Kruithof, A. Mol, C. J. G. Onderwater, R. W. Pattie, P. D. Shidling, M. Sohani, D. J. van der Hoek, A. Rogachevskiy, E. Traykov, O. O. Versolato, L. Willmann, H. W. Wilschut, and A. R. Young, Phys. Rev. Lett. **112**, 212301 (2014).
[13] X. Fléchard, E. Lienard, O. Naviliat-Cuncic, D. Rodriguez, M. A. G. Alvarez, G. Ban, B. Carniol, D. Etasse, J. M. Fontbonne, A. M. Lallena, and J. Praena, Phys. Rev. C **82**, 027309 (2010).
[14] O. Naviliat-Cuncic (private communication).
[15] A. Bacquias *et al.*, Eur. Phys. J. A **48**, 155 (2012).
[16] P. D. Shidling, D. Melconian, S. Behling, B. Fenker, J. C. Hardy, V. E. Iacob, E. McCleskey, M. McCleskey, M. Mehlman, H. I. Park, and B. T. Roeder, Phys. Rev. C **90**, 032501(R) (2014).
[17] J. Grinyer, G. F. Grinyer, M. Babo, H. Bouzomita, P. Chauveau, P. Delahaye, M. Dubois, R. Frigot, P. Jardin, C. Leboucher, L. Maunoury, C. Seiffert, J. C. Thomas, and E. Traykov, Phys. Rev. C **92**, 045503 (2015).
[18] G. Ban, D. Durand, X. Fléchard, E. Liénard, and O. Naviliat-Cuncic, Ann. Phys. **525**, 576 (2013).
[19] H. R. Glyde, J. Nucl. Mater. **23**, 75 (1967).
[20] V. Sciani and P. Young, Radiat. Eff. **78**, 87 (1983).
[21] http://faster.in2p3.fr
[22] Oscillator OCXS AOCJY5 from ABRACON, http://www.abracon.com/Precisiontiming/AOCJY5.pdf
[23] D. M. Webber, V. Tishchenko, Q. Peng, S. Battu, R. M. Carey, D. B. Chitwood, J. Crnkovic, P. T. Debevec, S. Dhamija, W. Earle, A. Gafarov, K. Giovanetti, T. P. Gorringe, F. E. Gray, Z. Hartwig, D. W. Hertzog, B. Johnson, P. Kammel, B. Kiburg, S. Kizilgul, J. Kunkle, B. Lauss, I. Logashenko, K. R. Lynch, R. McNabb, J. P. Miller, F. Mulhauser, C. J. G. Onderwater, J. Phillips, S. Rath, B. L. Roberts, P. Winter, and B. Wolfe, Phys. Rev. Lett. **106**, 041803 (2011).
[24] V. Horvat and J. C. Hardy, Nucl. Instrum. Methods A **713**, 19 (2013).
[25] C. Fontbonne Vanborren, Ph.D. thesis, Normandie Université, 2017 (unpublished), https://tel.archives-ouvertes.fr/tel-01467075
[26] https://www.r-project.org